Effect of solvent on the morphology and performance of cellulose triacetate membrane/cellulose nanocrystal nanocomposite pervaporation desalination membranes

by Indah Prihatiningtyas

Submission date: 17-Mar-2022 12:16PM (UTC+0700)
Submission ID: 1786154915
File name: effect_solvent_CRJ.pdf (9.53M)
Word count: 8532
Character count: 45897

Chemical Engineering Journal 388 (2020) 124216

Contents lists available at ScienceDirect

Chemical Engineering Journal

journal homepage: www.elsevier.com/locate/cej

Effect of solvent on the morphology and performance of cellulose triacetate membrane/cellulose nanocrystal nanocomposite pervaporation desalination membranes

Indah Prihatiningtyas[a,b], Yi Li[a], Yusak Hartanto[c], Anja Vananroye[d], Nico Coenen[d], Bart Van der Bruggen[a,e,*]

[a] Department of Chemical Engineering, KU Leuven, Celestijnenlaan 200F, Box 2424, B-3001 Leuven, Belgium
[b] Department of Chemical Engineering, Mulawarman University, Jalan Sambaliung No. 9, Sempaja Selatan, Samarinda, Kalimantan Timur, Indonesia
[c] Centre for Membrane Separations, Adsorption, Catalysis and Spectroscopy for Sustainable Solutions, KU Leuven, Celestijnenlaan 200F, Box 2454, 3001 Leuven, Belgium
[d] Soft Matter, Rheology and Technology, Department of Chemical Engineering, KU Leuven, Celestijnenlaan 200F, Box 2424, B-3001 Leuven, Belgium
[e] Faculty of Engineering and the Built Environment, Tshwane University of Technology, Private Bag X680, Pretoria 0001, South Africa

HIGHLIGHTS

- Effect of solvents on the morphology and performance of CTA/CNCs PV membranes.
- DMSO-based membrane resulted in the best pervaporation desalination performance.
- DMSO-based membrane had stable desalination performance at hypersaline condition.

GRAPHICAL ABSTRACT

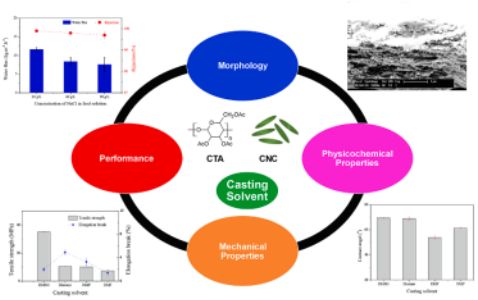

ARTICLE INFO

Keywords:
Solvent effects
Pervaporation
Desalination
Cellulose nanocrystals
Nanocomposite membrane

ABSTRACT

The effects of different solvents (dimethyl sulfoxide (DMSO), dioxane, 1-methyl-2-pyrrolidinone (NMP), and dimetylformamide (DMF)) on the morphology of nanocomposite membranes intended for pervaporation (PV) and on their desalination performance were investigated. Cellulose triacetate/cellulose nanocrystals (CTA/CNCs) nanocomposite PV membranes were successfully prepared via solution casting in different solvents, aiming to obtain the optimum solvent leading to the best desalination performance. The fabricated nanocomposite membranes were characterized to study the membrane crystallinity, chemical composition, morphology, surface hydrophilicity, mechanical properties, thermal stability and the membrane performance in pervaporation desalination process. DMSO as casting solvent resulted in a transparent PV nanocomposite membrane, while other solvents yielded opaque membranes due to the aggregation of CNCs on the CTA matrix. Among the four solvents, the DMSO-based membranes resulted in a hydrophilic nanocomposite membrane with homogeneously distributed CNCs on the membrane surface and the matrix with self-assembled structure. These membranes showed a high water flux of 11.67 kg m^{-2} h^{-1} without compromising NaCl rejection at the level of 99.9% in the feed solution of 30 g L^{-1} of NaCl. Furthermore, the CTA/CNCs-DMSO nanocomposite membranes also showed a good PV desalination performance for a highly saline feed (up to 90 g L^{-1} of NaCl) while other

* Corresponding authors at: Department of Chemical Engineering, KU Leuven, Celestijnenlaan 200F, Box 2424, B-3001 Leuven, Belgium.
E-mail addresses: indahprihatiningtyas.yamsidi@kuleuven.be (I. Prihatiningtyas), bart.vanderbruggen@kuleuven.be (B. Van der Bruggen).

https://doi.org/10.1016/j.cej.2020.124216
Received 22 October 2019; Received in revised form 22 January 2020; Accepted 24 January 2020
Available online 04 February 2020
1385-8947/

membranes suffered from salt penetration and membrane leakage for dioxane-based and NMP-based membranes, respectively. Therefore, DMSO as a green solvent has potential for fabricating CTA/CNCs PV nanocomposite membranes.

1. Introduction

The decreasing quality of available natural water resources due to water pollution, groundwater exploitation, and growing living standards, increase water consumption and lead to water scarcity. It has been predicted that more than one-third of the world's total population will endure the lack of potable water in the future [1,2]. Abundant water resources are available in the world but almost 97% is seawater [3], hence desalination is an emerging technology to overcome such water crisis.

Pervaporation (PV) is an attractive technology to be applied in desalination process due to its high salt selectivity. In addition, it is an environmentally friendly process, which is able to handle feed waters with high salinity and has limited effects of fouling [4]. Unfortunately, the permeability of current PV membrane processes is still relatively low compared to that of other membrane-based desalination processes, especially for cellulose-based PV membranes [5]. Cellulose triacetate (CTA), a derivative of cellulose, is widely used as membrane material due to its good mechanical strength, relative hydrophilicity, low fouling tendency, and high oxidation resistance. It can be prepared as a very dense film, which is necessary for their use as PV desalination membranes [6–8].

As a common strategy to improve membrane performance, polymer nanocomposite membranes prepared by blending hydrophilic nanofillers into polymer matrix have been employed [9–12]. Furthermore, incorporating hydrophilic nanomaterials has been proven to effectively tune the physicochemical properties of the membrane [9], such as surface hydrophilicity [13–15], Porosity [16], charge density [17], and thermal and mechanical properties [18]. Several examples of common nanomaterials that have been utilized to prepare desalination membranes [19,20], such as silica [21], zeolite [22], alumina, clay [23], TiO_2 [24], MoS_2 [25], graphene oxide [26], carbon dots [27], carbon nanotubes (CNTs) [28], and multi-walled carbon nanotubes (MWNTs) [29]. However, nanofiller aggregation still remains a persistent issue in the preparation of nanocomposite membranes via physical blending of polymers and nanomaterials [10]. Generally, there are two factors that cause poor dispersity of nanoparticles in polymer matrices, (1) incompatibility between polymer and nanoparticles and (2) high additive concentration, leading to the agglomeration of nanoparticles in the membrane matrix during phase inversion [10,30]. As a result, numerous studies focused on the modification of the surface of nanoparticles to improve the compatibility between nanofillers and the polymer matrix [31,32]. The surface modification process involves a complicated chemistry, resulting in an increase of the overall membrane preparation costs. On other hand, leaching out of nanoparticles into downstream has been highlighted with the drinking water safety regulation issued [33], hence using biocompatible nanoparticle has been interesting to be applied.

Recently, there has been an interest to apply cellulose nanocrystal (CNCs) as nanofillers in membrane preparation due to some additional benefits such as low cost, low density, and good mechanical properties. Furthermore, CNCs are renewable, non-toxic, and can easily undergo surface modifications [34,35], making this class of nanomaterials an attractive alternative to conventional inorganic nanofillers. In another study, Bai et al. prepared a novel thin film composite (TFC) nanofiltration membranes (CNC-TFC-Ms) by incorporated CNC into a polyamide (PA) layer. They reported that incorporation of 0.2 wt% CNCs increased water permeance by 57.1% (from 9.52 LMH bar^{-1} to 14.96 LMH bar^{-1}), while the NaCl rejection increased from 18% to 24% [36]. Liu et al. fabricated reverse osmosis (RO) membrane by oxidized cellulose nanofibers (CNFs) with 2,2,6,6-tetramethylpiperidine-1-oxyl radical (TEMPO), then modified CNFs incorporated into the polyamide layer of thin film composite (TFC) [37]. The water flux of the membrane enhanced by more than 50% to 29.8 L $m^{-2}h^{-1}$ at operating pressure of 1.5 MPa compared to that of the pristine RO membrane at loading of 0.02 wt% CNFs, while the NaCl rejection improved from 94.0% to 96.2% [37]. Asempour et al. fabricated TFN RO membrane by embedding CNCs into the polyamide active layer [33]. At loading of 0.1% (w/v), the desalination experiments at 20 bar showed doubling of the water flux from 30 L $m^{-2}h^{-1}$ to 63 ± 10 L $m^{-2}h^{-1}$, without significantly compromising the salt rejection (97.8%) [33]. Lately, Prihatiningtyas et al. fabricated the CNCs-cellulose triacetate (CTA) pervaporation (PV) nanocomposite membrane by solution casting method [38]. They reported that loading 3 wt% of CNCs into dope solution increased the water flux by a factor of 3, from 2.16 kg $m^{-2}h^{-1}$ to 5.76 kg $m^{-2}h^{-1}$. Moreover the water flux obtained of 11.68 kg $m^{-2}h^{-1}$ by reducing the casting blade height from 200 to 100 μm, while the NaCl rejection kept 99.9% [38]. Although Prihatiningtyas et al. did not study the effect of the solvent on the membrane performance.

Some solvents were used to prepare CTA membranes, such as N-methyl-2-pyrrolidone (NMP) [39], 1–4 dioxane [40,41], dichoromethane [42,43], dimethylformamide (DMF) [44], chloroform [45], and DMSO [38]. Limited information was available why such solvents had been used to prepare such membranes. Solvents have specific physicochemical properties, which will interact with both the polymer and the additives, resulting in different membrane morphologies and eventually also different membrane properties [46]. For example, a poor dispersion of CNCs within the polymer matrix will decrease the mechanical performance of the membrane [47]. Thus, understanding the role of different solvents used to prepare CTA/CNCs PV membranes would guide the membrane preparation.

In this work, the effect of different solvents on the physicochemical properties of nanocomposite CTA/CNCs PV membranes was investigated. Four common organic solvents, namely DMSO, dioxane, DMF, and NMP, were used in the preparation of the dope solution and dispersion of CNCs. The physical structure, surface hydrophilicity, surface chemistry and mechanical strength of the nanocomposite membranes were thoroughly characterized to understand the effect of the solvent on the physicochemical properties of the membrane.

2. Experimental

2.1. Chemicals and materials

Cellulose triacetate (CTA, acetyl content 43–44%, molecular weight 966.845 g/mol) was purchased from ACROS (China), dimethyl sulfoxide (DMSO, 99.5%, reagent) was obtained from Honeywell (Japan), and dimetylformamide (DMF, extra pure) was obtained from ACROS (USA). 1-Methyl-2-pyrrolidinone (NMP, 99%) was purchased from Honeywell (Germany) and 1–4 dioxane (stabilized) was purchased from J.T. Baker (the Netherlands). CNCs were purchased from CelluForce Inc. (Canada). Sodium chloride was obtained from VWR (Belgium) and was used as the solute in the feed solution during pervaporation. All chemicals were used without further purification.

2.2. Membrane preparation

CNCs suspensions were made by dispersing 3 wt% CNCs (with respect to the casting dope solution weight) in the different solvents

(DMSO, 1–4 dioxane, DMF and NMP). The physical properties of the solvents are listed in Table 1. According to the supplier, the CNCs powder has an aggregated particle size of 1–50 μm, a diameter of 2.3–4.5 nm and a length range of 44–108 nm. The CNCs suspensions were mixed with a magnetic stirrer for three hours. Next, 6 wt% CTA was added to the CNCs suspensions, followed by stirring for 15 h at 40 °C (NMP at 70 ^{0}C, due to the very slow dissolution at 40 °C). The casting dope solution was left for four hours at room temperature and was then cast on the glass plate using an automatic casting device with a casting blade height of 100 or 200 μm at room temperature with a relative humidity between 34 and 44%. The cast polymer films were dried in a vacuum oven for four hours at 60 °C and 5 inHg. Membrane characterization was conducted for membranes cast with 200 μm casting blade height, while for performance testing, membranes cast with a 100 μm casting blade height were used in view of their lower mass transfer resistance.

2.3. Characterization of the membrane

2.3.1. Viscosity

The polymer dope solution viscosities was examined by a stress-controlled rheometer (Anton Paar MCR501) with peltier system (P-PTD200) to control measurement temperature. A cone-plate geometry of 50 mm with cone angle of 1° was used for measuring the less viscous samples, whereas a cone-plate geometry of 25 mm and 4° cone angle was applied for the highly viscous samples (viscosities above 10 Pa.s). Viscosity as a function of shear rate was probed in steady shear flow [from 0.01 to 10 1/s with 5 data points per decade]. The RheoPlus software (Anton Paar GmbH, Austria) was used for collecting the data and analysis.

2.3.2. X-ray diffraction (XRD)

X-ray analysis was done on CNCs powders, pristine CTA membranes, and CTA/CNCs nanocomposite membranes using a Philips PW1830 diffractometer with Bragg/Brentano θ–2θ setup, CuKα radiation at 45 kV–30 mA on 173 mm goniometer circle, within the scan range of 3–75°(Rietveld users), for 1 h.

2.3.3. Scanning electron microscopy (SEM)

The surface and the cross-section morphologies of the composite membranes were observed with a XL30 FEG field-emission scanning electron microscope (FE-SEM, Netherlands) after being sputter-coated with a 1.5–2 nm gold layer. The samples were prepared by fracturing the membranes in liquid nitrogen liquid before cross-section imaging. A voltage of 10 kV was used to attain the surface and the cross-section images.

2.3.4. Fourier transform infrared (FTIR)

The chemical composition of the CTA powder, solvents, and the CTA/CNCs composite membranes were analyzed by Fourier transform infrared spectroscopy (FTIR, PE spectrum 100 with universal ATR sampling accessory, USA).

2.3.5. Contact angle

Contact angle measurements were conducted using a standard contact angle apparatus (Krüss GmbH Germany, model: DSA 10-Mk2) to determine the degree of wettability. The measurements were performed using a drop-shape analysis software. A syringe plunger was utilized for drop depositions on the surface of the membrane under study at room temperature. The liquid water volume was set at 2 μl at a rate of 24.79 μl/min.

2.3.6. Mechanical properties

The modulus of elasticity and tensile strength of the CTA/CNCs composite membranes were determined using a mini tensile/compression machine (model: Instron 5943). The samples were snipped into a square shape with width of 10 mm and length of 10 mm in ambient condition, at least four specimens were tested for each nanocomposite membrane.

2.3.7. Thermal gravimetric analysis (TGA)

Thermal stability of the CTA/CNCs composite membranes was investigated by a thermo-gravimetric analyzer (TGA Q500, TA Instruments, USA), in nitrogen atmosphere (40 ml/min), with a ramp of 10 °C/min from room temperature to 550 °C.

2.3.8. Particle size analysis

Particle size of CNCs in the suspensions were analyzed by a particle analyzer (Nanoplus 3-Zeta/nano particle analyzer, USA). The Nanoplus has a dynamic sizing range of 0.1 nm to 12.30 μm in a concentration range of up to 40% w/v, and a sensitivity for molecular weight to as low as 250 Da.

2.4. Performance of the membrane: water flux and rejection

The membrane performance was investigated using a customized setup, schematically shown in Fig. 1. A vacuum pump (Edwards two stage model E2M2, vacuum pressure 0.1–1 mbar) was employed on the permeate side to create a vapor pressure difference across the membranes. Pervaporation was operated at 70 °C with a feed solution of 30–90 g L^{-1} NaCl in DI water, at a feed flow rate of 70–80 L h^{-1}, and with an effective membrane surface area of 19.625 cm^2 (diameter = 5 cm). Each PV experiment took at least two hours and the permeate samples were collected at predetermined time interval and were weighed. The water flux J_w (kg m^{-2} h^{-1}) was determined by the following equation:

$$J_w = \frac{m}{(A.\ t)} \tag{1}$$

where m is the mass of permeate obtained (kg), A is the membrane area (m^2) and t is the working time (h). The salt rejections R (%) were calculated from the following equation:

$$R(\%) = 100\left(1 - \frac{C_p}{C_f}\right) \tag{2}$$

Table 1
Physical properties of organic solvents used to prepare CNCs/CTA dope solutions.

Solvent	Boiling point (°C)	Viscosity (η,cP, 20 °C)	Mole volume (Vm, cm^3 mol^{-1})	Hansen solubility parameter (MPa$^{1/2}$)			
				δd, (MPa$^{1/2}$)[a]	δp, (MPa$^{1/2}$)[a]	δh, (MPa$^{1/2}$)[a]	δsp, (MPa$^{1/2}$)[b]
DMSO	189	2.24	71.3	18.4	16.4	10.2	26.7
Dioxane	101	1.37	85.7	19	1.8	7.4	27.2
DMF	153	0.92	77	17.4	13.7	11.3	24.9
NMP	202	1.67	96.5	18	12.3	7.2	23

[a]: Hansen Solubility Parameters: A User's Handbook (second edition), page 429–471.
[b]: Calculate according to the equation $\delta sp = \sqrt{\delta d^2 + \delta p^{2+} \delta h^2}$.

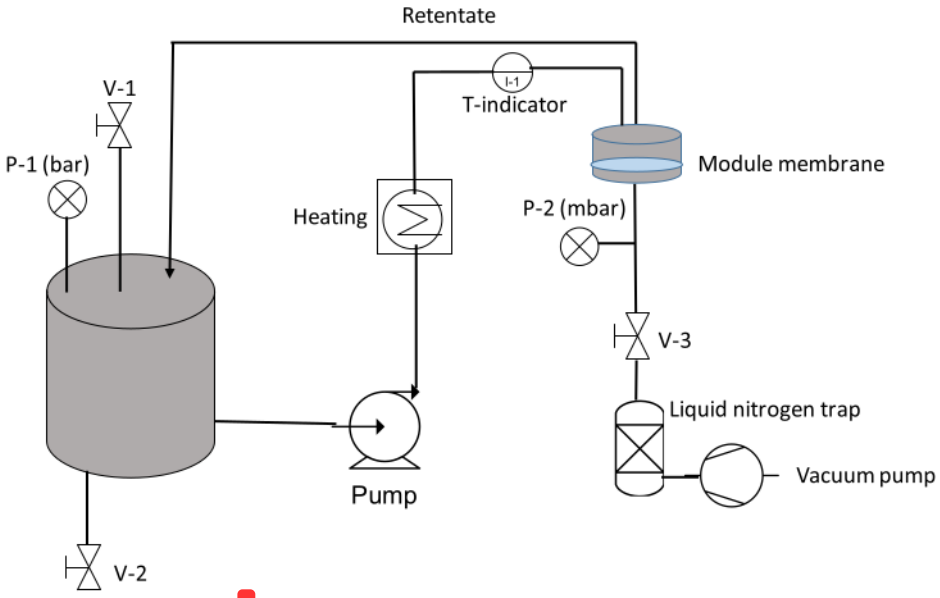

Fig. 1. Schematic diagram of the experimental setup for pervaporation.

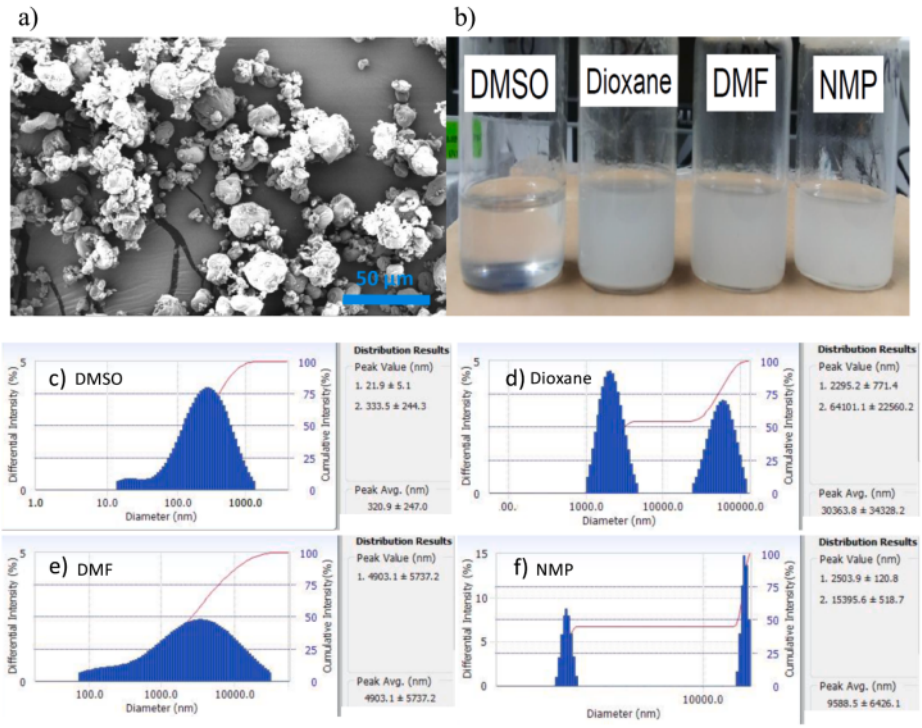

Fig. 2. (a) SEM image of CNCs powder. (b) Photographs of the CNCs suspension in the different casting solvents. (c-f) Particle size distribution of CNCs in different casting solvents.

where c_p and c_f are the salinity in the permeate and feed solutions, respectively. The salinity of water was determined by a Consort model C831-conductivity meter. The calibration curve of the conductometer is shown in Fig. S1.

3. Results and discussion

3.1. Effect of different solvents on membrane morphology

Fig. 2a shows the Scanning Electron Microscope (SEM) image of CNCs powder. The particle size of the commercial CNCs has a wide distribution with a range of 1–24 μm. Four organic solvents (DMSO, 1–4 dioxane, DMF, NMP) were selected to disperse the CNCs at a 3 wt% concentration. It was found that DMSO had an excellent dispersibility for CNCs, which could be concluded from the transparent feature of the dispersion, as shown in Fig. 2b. However, the dispersion of CNCs in the other three solvents had a milky and non-transparent appearance. Precipitation of CNCs in 1–4 dioxane and only a moderate dispersibility of CNCs in DMF and NMP was observed. This indicates that CNCs disperses more preferentially in DMSO compared to the other three solvents. Particle size analyzer was further used to examine the CNCs particles sizes in different solvents.

As shown in Fig. 2c, the CNCs have an apparent mean particle size of 320.9 nm in DMSO. This nanoscale particle dimension is significantly lower than the original particle size of CNCs which is in the micrometer range, as can be observed in Fig. 2a. The reduced particle size and the narrow size distribution of CNCs in DMSO imply that the CNCs aggregates are broken down into separated particles with a good stability in DMSO. When dispersed in DMF, CNCs aggregates have a broad particle size distribution and a larger apparent mean particle size (4.9 μm) while two peaks are observed for CNCs dispersed in both dioxane and NMP (Fig. 2d, f). In addition, even larger CNCs mean particle sizes were observed compared to CNCs dispersed in DMSO and DMF. It is concluded that the compatibility and dispersibility of these four solvents for the CNCs are in the sequence of DMSO > DMF > NMP > dioxane. The main reason that CNCs can be dispersed in DMSO is due to the highest polarity value of DMSO (δp = 16.4 $MPa^{1/2}$) compared to the other solvents (Table 1). CNCs are considered to be a polar material with surface charge and electrostatic repulsion interactions between the CNCs rods [48]. As a result, CNCs will develop a better interaction with a solvent which has a high solubility parameter through ion–dipole interactions. DMSO might donate a strong ionic strength in the suspension, of which the resulting repulsion prevents aggregation. In contrast, the weak ionic strength of dioxane leads to the agglomeration of CNCs (δp = 1.8 $MPa^{1/2}$).

Apart from the dispersion quality of CNCs, the solvent also played an important role to determine the viscosity of polymer dope solution. Theoretically, the viscosity of the casting solution has a great influence on the mixing of components (polymer, solvent, additives) as well as the phase transition during the membrane fabrication process, thereby affecting the final membrane morphology. The viscosity of a solution depends on numerous parameters, including temperature, the solvent properties, the polymer concentration, molecular weight and molecular weight distribution [49]. In this work, the temperature was fixed at 27 °C (room temperature in the membrane preparation laboratory), the CTA polymer (molecular weight: 966.845 g mol^{-1}) was added in a concentration of 6 wt% to each of the 3 wt% CNCs suspensions. These suspensions were prepared using different solvents (DMF, DMSO, NMP, dioxane). The physicochemical properties of solvents used in this work are given in Table 1.

Fig. 3 shows the viscosities of the prepared dope solutions as a function of shear rate. The viscosity of the casting dope solution prepared using DMF is the highest in a shear rate range from 0.05 to 5 1/s compared to that of dope solution prepared using DMSO, NMP, and dioxane. This is ascribed to the fact that DMF has the highest hydrogen bond interactions between the solvent and CTA by considering the δ_h = 11.13 $MPa^{1/2}$, followed by DMSO (δ_h = 10.2 $MPa^{1/2}$), dioxane (δ_h = 7.4 $MPa^{1/2}$), and NMP (δ_h = 7.2 $MPa^{1/2}$). The viscosity reflects the interaction between the polymer and the solvent caused by swelling of the macromolecules through hydrogen bonding. The polymer chains become disconnected and elongated when the polymer is dissolved in a solvent and thus increasing the dope solution viscosity due to solvent hydrodynamic volume enhancement [50]. The viscosity is assumed to have an influence on the membrane morphology since a more viscous dope solution will slow down the exchange between solvent and non-solvent during phase inversion process.

The choice of solvent also has an impact on the final optical appearance of the membranes. CTA/CNC_S nanocomposite membranes fabricated with DMSO (CTA/CNCs-DMSO) are transparent while DMF-, dioxane- and NMP-based membranes have an opaque appearance, as

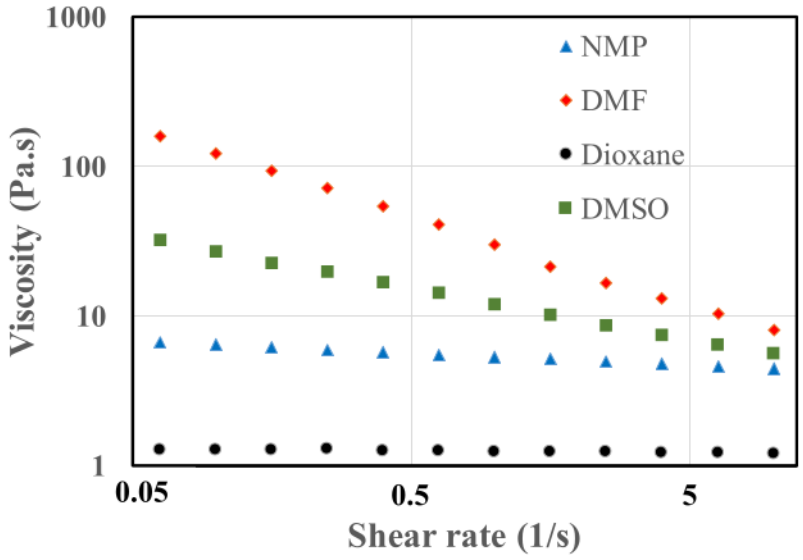

Fig. 3. CTA/CNCs casting dope viscosity in different casting solvents.

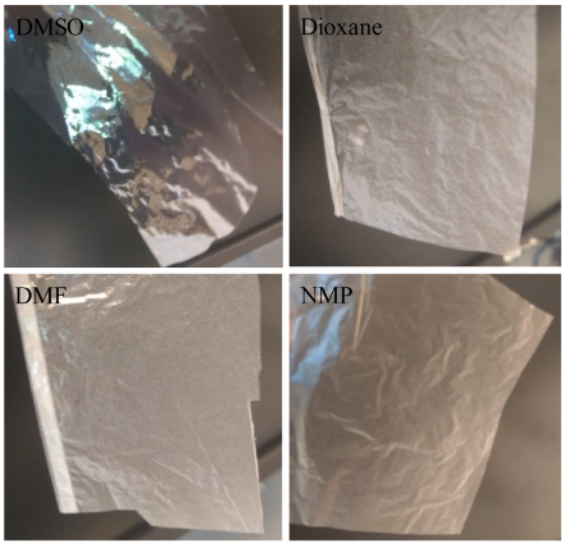

Fig. 4. Photograph of nanocomposite CTA/CNCs membranes fabricated from different solvents (a), the final thickness of the membranes (b).

shown in Fig. 4a. This could be attributed to the poor dispersion quality of CNCs in the latter three solvents. Fig. 4b also reveals that the final thickness of the DMF-, dioxane- and NMP-based membrane are higher than DMSO-based membrane due to the poor dispersion which leads to an aggregation of CNCs in the CTA membrane.

Fig. 5 shows the different membrane surface and cross-section morphologies using different solvents. The incorporation of CNCs into the CTA polymer results in nanocomposite membranes with a unique self-assembled structure (e.g. Fig. 5g), while the pristine CTA membrane has a sponge-like structure (Fig. 5f). Fig. 5b indicates that the surface of the CTA/CNCs-DMSO nanocomposite membrane is the smoothest among all solvents containing CNCs, which is consistent with the finding that CNCs can be well dispersed in DMSO as indicated by the transparent CNCs dispersion in DMSO in Fig. 2b and the transparent membrane in Fig. 4a.

The cross-section image shown in Fig. 5i reveals that the CTA/CNCs-DMF nanocomposite membrane has the most solid and compact structure compared to membranes produced using other solvents, due to the high viscosity of the DMF-based dope solution (Fig. 3). A higher dope solution viscosity slows down the solvent exchange during the phase inversion process. This reduces the driving force for membrane precipitation, resulting in a solid and compact morphology.

X-ray diffraction (XRD) was used to characterize the presence of CNCs in the membrane and the stability of the CNCs crystalline structure. As shown in Fig. 6, the pristine CNCs with a well-defined crystal structure has typical peaks at 15°, 22° and at 34° while the pristine membrane without CNCs showed a single characteristic peak at 8.5°. Fig. 7 presents the XRD spectra of CTA/CNC nanocomposite membranes fabricated from different solvents. For all CNC containing CTA membranes, a peak at 8.5° can be seen, similar to the pristine CTA membrane. In addition, the CNCs crystalline structure was observed in all membranes fabricated from different solvents with a characteristic peak at 22°, which is related to crystallographic planes [51]. Also, the intensity level of this characteristic peak for membrane prepared from different solvent can be clearly differentiated from the XRD pattern; the peak intensity level at 22° shows the following sequence: DMSO > DMF > NMP > 1–4 dioxane. A higher intensity indicates a better dispersion (and hence a better dispersing solvent), because a well-defined structure has a higher crystallinity [51]. It can be concluded that DMSO is the optimal solvent for the dispersion of CNCs in the dope solution.

The surface functional group characterization of CTA/CNCs nanocomposite membranes casted from different solvents by FTIR is shown in Fig. 8. The most characteristic peaks for CNCs and CTA are mostly similar because these two compounds are cellulose-based materials. The peaks at 3340, 2901, 1430, and 1059 cm^{-1} correspond to O–H, C–H, $–CH_2$, and C–O, respectively [52], which shows the chemical functional groups of CNCs.

The peak at 1742 cm^{-1} corresponds to C=O stretching, the peak at 1365 cm^{-1} is related to the asymmetric bending of C–H, the peak at 1217 cm^{-1} is attributed to the C-O stretching, the peak at 1030 cm^{-1} belongs to pyranose ring C–O–C stretching (Fig. 8a), and the peak at 3340 cm^{-1} corresponds to the O–H stretching (Fig. 8b). The characteristic peak at 1109 cm^{-1} (C–O) in Fig. 8a and the broad peaks at 3477–3600 cm^{-1} (O–H) in Fig. 8b are only observed in DMSO, probably due to hydrogen bonding between CTA and CNC. However, the characteristic peaks of the solvent are not present in the FTIR spectra because the solvent was evaporated.

As pervaporation membrane generally has a dense structure and the separation mechanism based on the solution-diffusion mechanism, the diffusion rate will depend on the permeant solubility, which has a direct relationship on the interaction between the permeant and the membrane material [53]. To probe this interaction, Fig. 9 presents the contact angle values of water on CTA/CNCs nanocomposite membranes fabricated from different solvents. Membrane surface with high hydrophilicity, represented by low contact angle, is deemed important to enhance the transport of water molecules in the membrane matrix.

All membranes were found to be hydrophilic with a contact angle between 50 and 70°. The nanocomposite membranes fabricated from DMSO and dioxane have a similar contact angle around 69.5°, while the NMP-based membranes have an even lower contact angle than the former membranes (60°). However, membranes prepared from DMF show the lowest water contact angle (53.8°). The hydrophilicity/hydrophobicity is mainly affected by the combination of surface morphology and the surface chemistry. The higher hydrophilicity of membranes prepared from DMF can be ascribed to the large content of O–H groups on the membrane surface (see Fig. 8b), originating from the trace amount of DMF which cannot be completely removed during solvent evaporation process.

The dense nature of PV membrane requires the membrane thickness is kept to be as thin as possible to reduce transport resistance while maintaining satisfactory mechanical properties during operational process. For this reason, the tensile strength and elongation of CTA/CNCs nanocomposite membranes cast different solvents were measured and the results are shown in Fig. 10.

CNCs have been used as a reinforcement for numerous polymer nanocomposites. A good dispersion quality of the CNCs in the dispersant and within polymer matrix are desirable to reinforce the final nanocomposite membrane. On the other hand, CNCs agglomeration is to be avoided since it will compromise membrane mechanical properties [54]. Compared with inorganic nanofillers, CNCs have better degree of dispersion in polymer matrix because of the superior interactions between CNCs and polymer chains. Fig. 10 shows that the CTA/CNCs nanocomposite membrane fabricated with DMSO has the highest tensile strength, due to the good dispersion of the CNCs, which create a positive interface between CTA matrix and CNCs. A better interfacial adhesion between the CNCs and CTA obtains due to the strong bonding and great interface, hence, the stress can shift to the CNCs efficiently then the break strength can be higher [55]. Nanocomposite membranes fabricated with dioxane, DMF and NMP, have a lower membrane strength, mainly caused by the high degree of agglomeration of CNCs in the membrane (Fig. 5).

The thermal stability is another important factor for the PV membrane as PV separation is a thermally-driven process. Thermal properties of CTA/CNCs nanocomposite membranes prepared from different solvents were observed by Thermal Gravimetric Analysis (TGA), as shown in Fig. 11. The results show a slight difference between the TGA

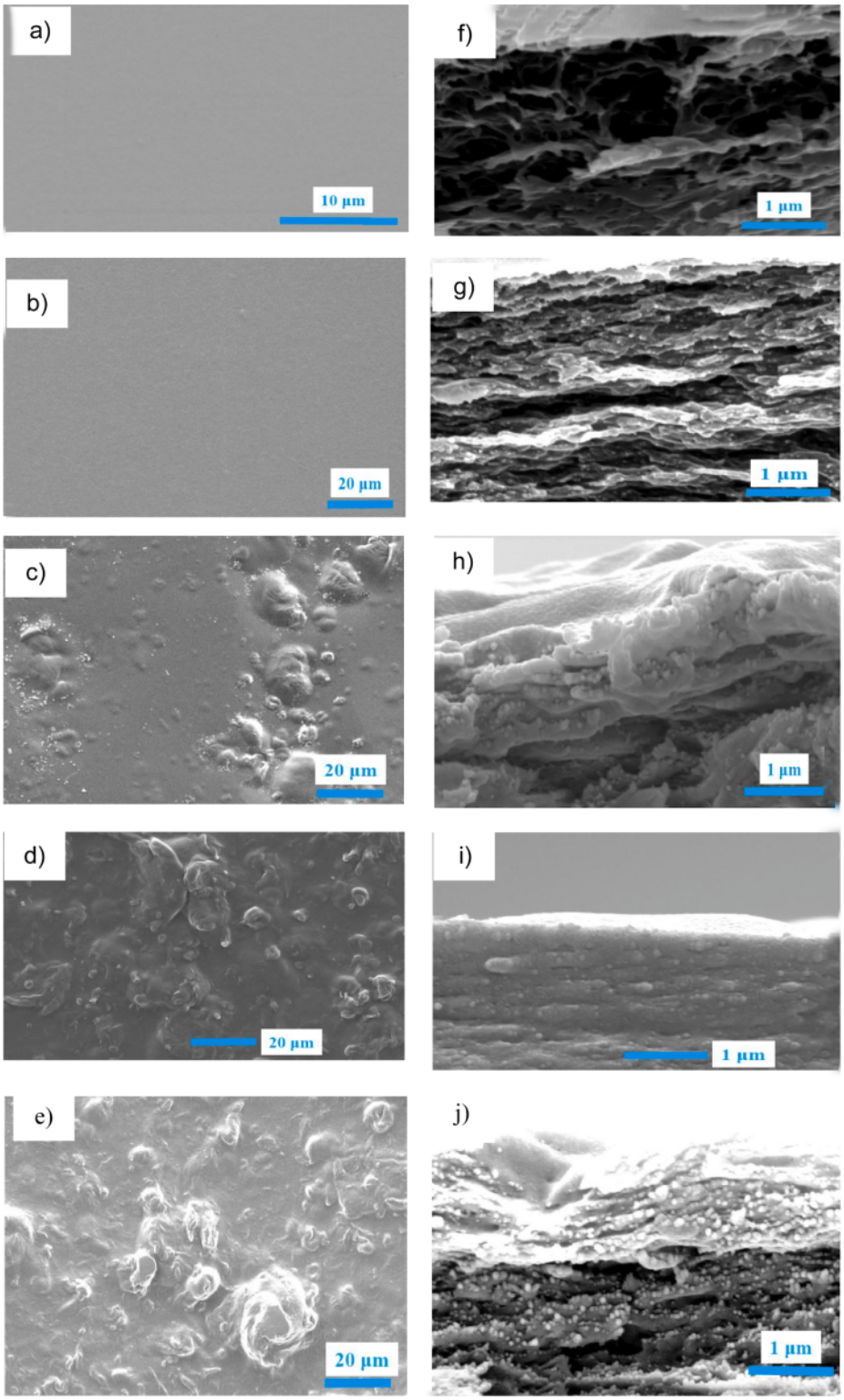

Fig. 5. SEM images of membrane surface (a–e) and cross-section (f-j) of a) Pristine CTA membrane in DMSO. b) CTA/CNCs-DMSO nanocomposite membranes. c) CTA/CNCs-dioxane nanocomposite membranes. d) CTA/CNCs-DMF nanocomposite membranes. e) CTA/CNCs-NMP nanocomposite membranes.

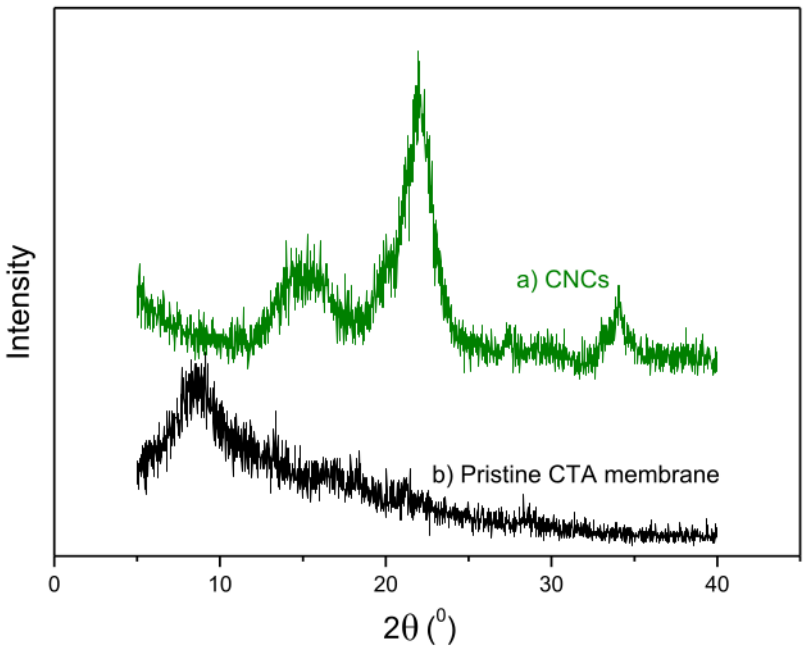

Fig. 6. X-ray diffraction, a) CNCs, and b) pristine CTA membrane.

curves of the membranes developed in this study, but the pristine CTA membrane is very different. The weight loss at temperatures below 240 °C is ascribed to the evaporation of residual moisture or solvent. The thermal degradation of the CTA chain occurs at temperatures of 240–370 °C. The carbonization and the decomposition of the composite membranes take place at temperatures above 370 °C. The residue yield from CTA/CNCs nanocomposite membranes increases in comparison to the pristine CTA membrane, which is due to the CNCs increasing the char formation. The pristine CTA membrane has a different thermal degradation: the temperatures are in the range 300–370 °C. The presence of CNCs in the CTA membrane decreases the thermal degradation temperature due to the large number of free end chains in the CNCs

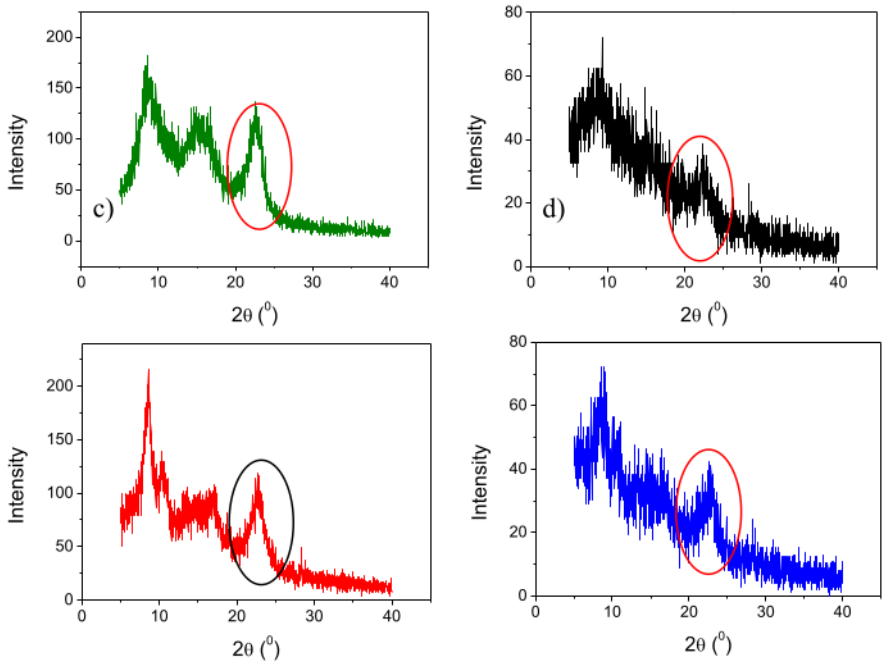

Fig. 7. X-ray diffraction of CTA/CNCs nanocomposite membranes fabricated from different solvents; a) DMSO, b) 1–4 dioxane, c) DMF, and d) NMP.

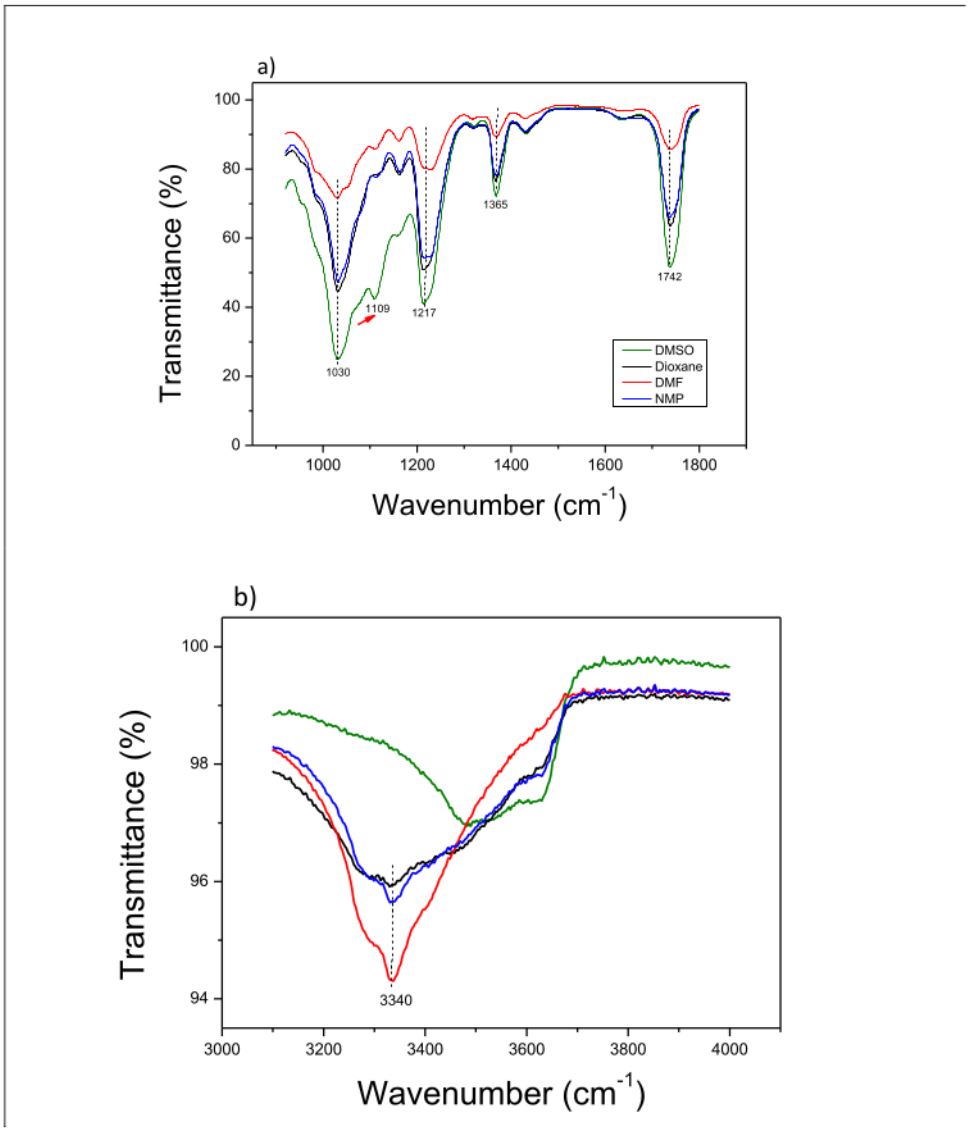

Fig. 8. FTIR spectra of CTA/CNCs nanocomposite membranes fabricated from different solvents, a) Wavenumber range in 1000 to 1800 cm^{-1}, and b) Wavenumber range in 3000–4000 cm^{-1}.

surface, starting to decompose at low temperatures [56,57]. However, thermal analysis studies suggest that all CTA/CNCs nanocomposite membranes have a sufficient thermal stability to tolerate the temperatures required for PV desalination, as PV operates at a feed temperature ranging from 30 to 90 °C.

3.2. Performance of CTA/CNCs nanocomposite membranes in pervaporation

Fig. 12 shows the membrane permeability and NaCl rejection of nanocomposites membranes prepared from different solvents.

The PV performance was evaluated using a feed solution with a concentration of 30 wt% NaCl at a temperature of 70 °C. Fig. 12 shows that a higher water flux is obtained with CTA/CNCs nanocomposite membranes fabricated with dioxane, NMP, and DMSO than for DMF-based membrane. The water fluxes for dioxane-based, NMP-based and DMSO-based membrane are 11.99, 11.68, and 11.67 kg $m^{-2}h^{-1}$ respectively. The lower water flux (8.08 kg $m^{-2}h^{-1}$) of DMF-based membrane can be related to the dense structure of the membrane, as observed in cross-sectional SEM image (see Fig. 5i). The dense structure hampers the water to penetrate in the membrane, giving rise to a lower water flux. The other membranes, with relatively loose intermediate layers, have a higher water flux. Interestingly, all the CTA/CNCs nanocomposite membranes exhibit a very high NaCl rejection, which remain above 99% due to the dense structure on the membrane surface as a selective layer. To further verify this behavior, the porosities of different membrane prepared from different casting solution was calculated and the results are summarized in Table 2. It can be concluded that there is no direct correlation between membrane porosities and pervaporation performance since the most dense membrane, such as

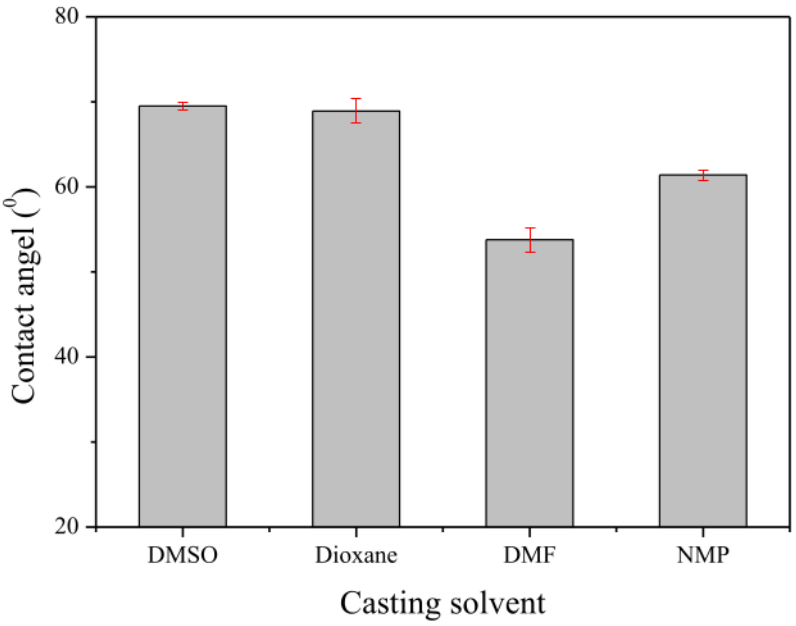

Fig. 9. Contact angle of water on CTA/CNC nanocomposite membranes fabricated from different solvents.

DMSO-based membrane still has comparable water flux to other membranes. The transport behavior of water molecules and sodium chloride are dependent on the membrane cross-section morphology.

Further investigation of the membrane performance was conducted by increasing the NaCl concentration in the feed. First, a high NaCl concentration (60 g L^{-1}) was used. The CTA/CNCs-NMP nanocomposite membrane was leaking during the PV desalination experiments (Video 1), whereas a slightly increased water flux was observed for CTA/CNCs-dioxane compared to the feed solution with 30 g L^{-1} of NaCl (from 11.99 kg $m^{-2}h^{-1}$ to 13.02 kg $m^{-2}h^{-1}$). Although the NaCl rejection of the CTA/CNCs-dioxane nanocomposite membrane can be maintained above 99%, NaCl crystallization occurred on the bottom of the spacer (permeate side) and membrane module, as shown in Fig. 13a-b. These leaking and salt penetration phenomena can be explained by concentration polarization effects, which usually occurs at high feed salinity, and will have serious effects on membrane lifetime [59].

As shown in Fig. 10, both the CTA/CNCs-dioxane and the CTA/CNCs-NMP nanocomposite membranes have a lower tensile strength due to aggregation of CNCs within the CTA matrix (see Fig. 5c and 5e). This compromises the stability of the CTA/CNCs-NMP nanocomposite

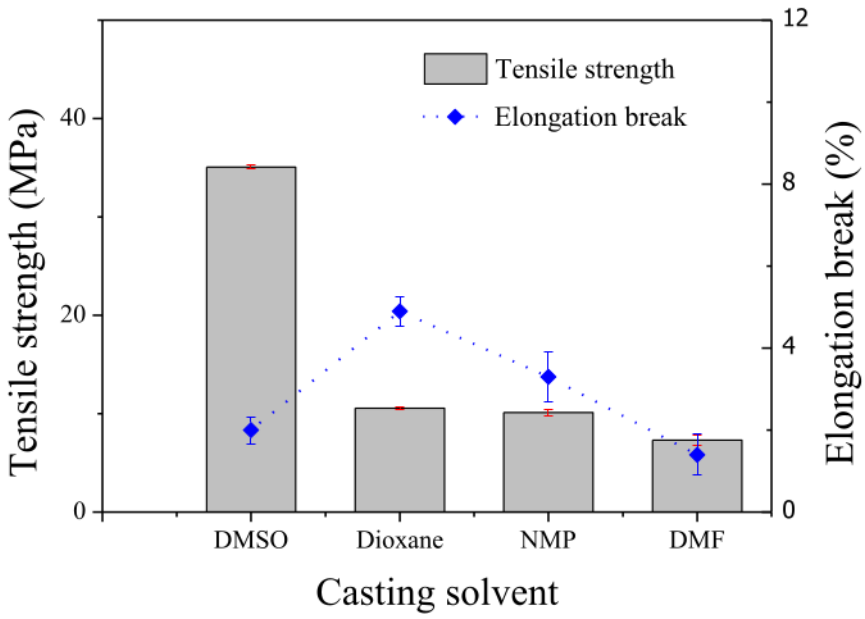

Fig. 10. Mechanical properties of CTA/CNCs nanocomposite membranes fabricated from different solvents.

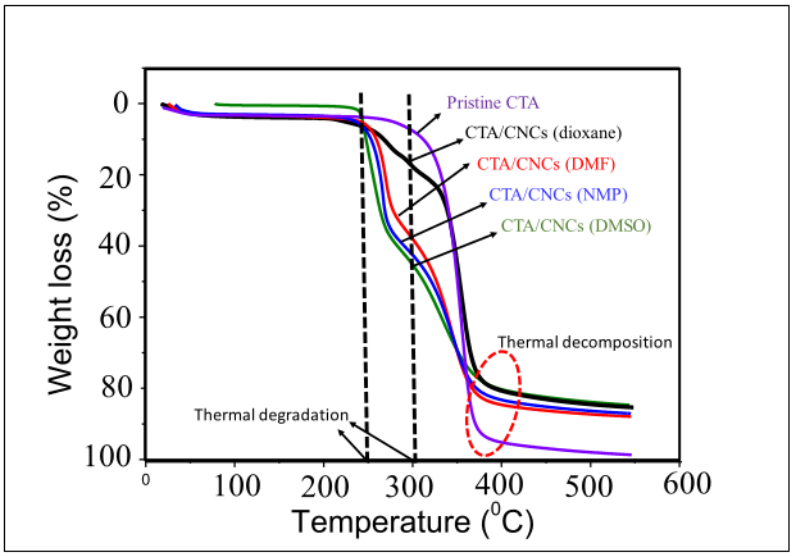

Fig. 11. TGA curve of CTA/CNCs nanocomposite membranes fabricated from different solvents.

membrane at high NaCl concentration polarization, i.e., the membrane is easily broken. For the CTA/CNCs-dioxane membrane, NaCl can penetrate to the membrane and be deposited on the spacer (permeate side), possibly due to weak interactions of CNCs and the CTA matrix, creating a defective membrane. The membranes used after PV desalination experiments for 60 g L^{-1} of NaCl in the feed solution are shown in Fig. S2. Among fabricated CTA/CNCs membranes, only CTA/CNCs-DMSO based membrane could survive during PV desalination process with 90 g L^{-1} of NaCl in feed solution as there was no salt on the spacer and membrane module (see Fig. 13c-d).

As shown in Fig. 14, the CTA/CNCs-DMSO nanocomposite membrane exhibits a better PV performance, even for a higher salinity feed solution, compared to CTA/CNCs-NMP and CTA/CNCs-dioxane membrane. The graph reveals a decrease in water flux of 28%, from 11.67 kg $m^{-2}h^{-1}$ to 8.4 kg $m^{-2}h^{-1}$ when the NaCl concentration in the feed increases from 30 g L^{-1} to 60 g L^{-1}. Increasing the NaCl concentration in the feed solution from 30 to 60 g L^{-1} relates to a decrease of the water concentration from 97 to 94 wt%. Hence, the solubility of water in the membrane decreases, which entails a decline of the driving force for the diffusion of water molecules in the membrane [60]. The increase of NaCl concentration in the feed solution could lead to a decrease of the vapor pressure at the feed side, leading to a reduced driving force and water permeation rate [61]. Other possible factors causing the water flux to decrease is concentration

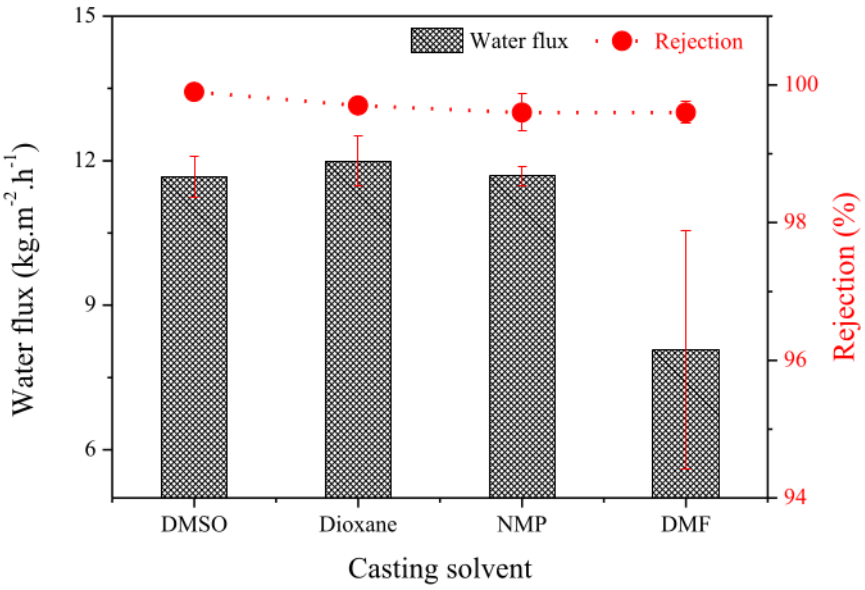

Fig. 12. Pervaporation performance of CTA/CNCs nanocomposite membranes fabricated from different solvents.

Table 2
The bulk porosity of the membranes.

Membrane type	Thickness (10^{-4} cm)	Membrane volume (cm^3)	Bulk porosity[a] (%)
CTA/CNCs-DMSO	6	0.0024	4.2
CTACNCs-DMF	21	0.0084	9 ± 0.008
CTA/CNCs-dioxane	21	0.0084	11 ± 0.007
CTA/CNCs-NMP	19	0.0076	17 ± 0.007

[a] Calculated based on bulk porosity method [58].

polarization on the membrane surface. An increase of the NaCl concentration at the membrane interface may interfere with the thermodynamic activity of water, thereby reducing the affinity of water molecules with the membrane polymers [6].

When the feed salinity was increased from 60 g L^{-1} to 90 g L^{-1}, no significant water flux decrease was seen. The water flux decreased by 7% (from 8.4 kg $m^{-2}h^{-1}$ to 7.6 kg $m^{-2}h^{-1}$) with a slight decline of NaCl rejection from 99.8 to 99.7%. The decrease of NaCl rejection could be caused by the diffusion of hydrated salt ions, which then condensed together with permeating water vapor [61]. Moreover, the increasing NaCl concentration leads to concentration polarization on the membrane surface, which may facilitate the salt to diffuse through the membrane.

The PV desalination performance of the CTA/CNCs-DMSO nanocomposite membrane was compared to other PV cellulose-based membranes for desalination, as listed in Table 3. The CTA/CNCs-DMSO nanocomposite membrane presents better pervaporation performance than those in previous study as listed in Table 3. The PV desalination performance obtained a higher water flux compared to Prihatiningtyas et al. [62] due to the thickness of CTA/CNCs-DMSO was thinner than CTA/Al_2O_3 membrane. Lonsdale et al. reported that in solution-diffusion theory which modeled by Fick's law stated that the flux of a species through the membrane is contrariwise proportional to the membrane thickness [63].

4. Conclusions

Four kinds of organic solvents (DMSO, dioxane, DMF and NMP) were utilized to investigate the effects of solvent on the physicochemical properties and pervaporation performance of CTA nanocomposite membranes with the incorporation of CNCs. The dispersion ability of the solvents for the CNCs followed the sequence DMSO > DMF > NMP > dioxane. The solvent had different effects on the membrane physicochemical properties. For example, due to the lower dispersibility of the CNCs in dioxane, membrane fabricated from dioxane presented a heterogeneous structure, a low crystallinity of the membrane matrix as well as a poor tensile strength. The use of DMF endowed the membrane with a higher membrane surface hydrophilicity but a lower tensile strength and dense intermediate layers. In comparison, the CTA/CNCs-DMSO nanocomposite membrane showed a more homogeneous membrane surface, a higher crystalline structure and a higher tensile strength. In PV experiments, the membrane fabricated from DMSO with a well-defined structure had a higher water flux (11.67 kg $m^{-2}h^{-1}$) and an excellent salt rejection (99.9%). Moreover,

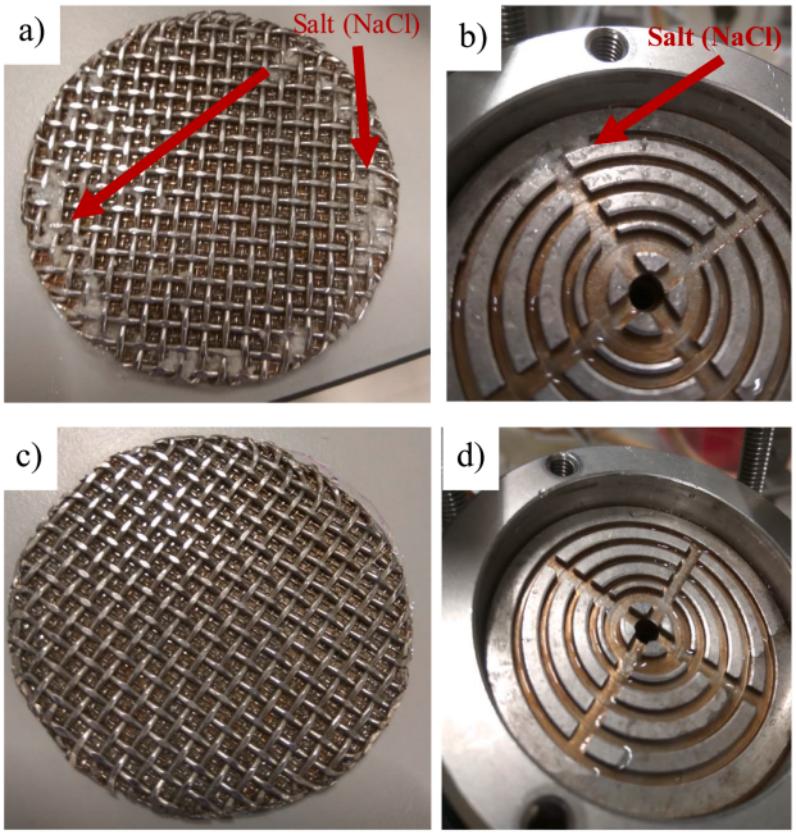

Fig. 13. Penetration of NaCl on the CTA/-dioxane nanocomposite membrane for 60 g L^{-1} of NaCl in feed solution (a-b), No penetration of NaCl on on the CTA/-DMSO nanocomposite membrane for 90 g L^{-1} of NaCl in feed solution (c-d).

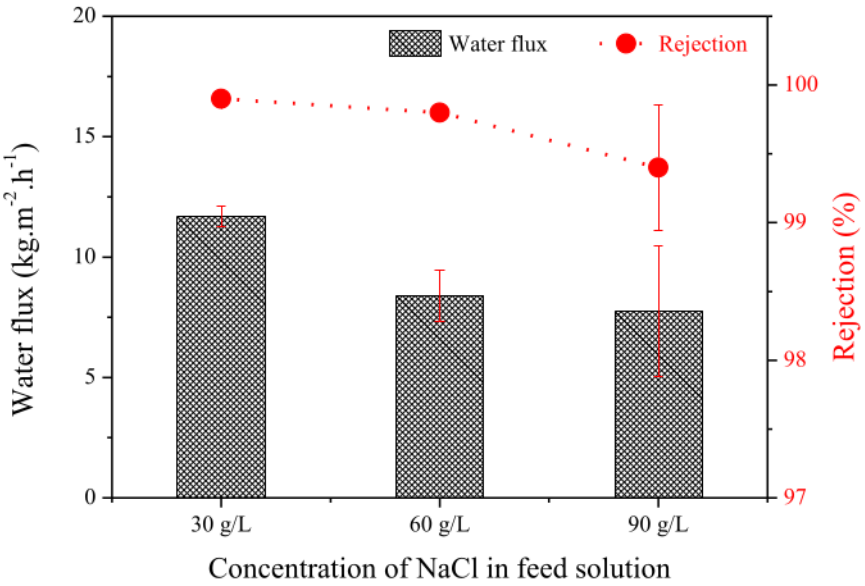

Fig. 14. Pervaporation performance of CTA/CNCs-DMSO nanocomposite membrane at different NaCl concentrations.

Table 3
Comparison the pervaporative desalination performance with previous cellulose based PV membranes.

Membrane	Temperature in feed side (^{0}C)	Conditions on permeate side	NaCl conc. (g/L)	Membrane thickness (μm)	Flux (kg/m^2.h)	NaCl rejection (%)	Ref.
Cotton cellulose	40	Vacuum	40	30	4.55–6.7	–	[64]
Cellulose diacetate on PTFE	40	Vacuum	40	3.5	4.5–5.1	–	[64]
Cellulose triacetate	50	Air sweep	100	10	2.3	99	[6]
Cellulose acetate	70	Vacuum	40–140	20–25	5.97–3.45	99.7	[65]
Cellulose triacetate/Al_2O_3	70	Vacuum	30–90	13	6.8–5	99.8	[62]
Cellulose triacetate/CNCs	70	Vacuum	30–90	6	11.67–7.6	99.7	This study

the CTA/CNCs-DMSO nanocomposite membrane also had a good PV desalination performance for a highly concentrated feed solution (90 g L^{-1}), which out-performs nanocomposite membranes prepared from dioxane and NMP. Selecting a good solvent is important in the fabrication of nanocomposite membranes due to its effects on the membrane morphology and therefore, on the pervaporation performance.

Declaration of Competing Interest

The authors declare that they have no known competing financial interests or personal relationships that could have appeared to influence the work reported in this paper.

Acknowledgements

This work was supported by the Indonesia Endowment Fund for Education (LPDP) Scholarship.

Appendix A. Supplementary data

Supplementary data to this article can be found online at https://doi.org/10.1016/j.cej.2020.124216.

References

[1] S.P. Dharupaneedi, S.K. Nataraj, M. Nadagouda, K.R. Reddy, S.S. Shukla, T.M. Aminabhavi, Membrane-based separation of potential emerging pollutants, Sep. Purif. Technol. 210 (2019) 850–866.
[2] M. Elimelech, W.A. Phillip, The future of seawater desalination: energy, technology, and the environment, Science 6043 (333) (2011) 712–717.
[3] E. Hameeteman, Future Water (In) security : Facts, Figures, and Predictions Future Water (In) Security : Facts, Figures, and Predictions, Glob. Water Inst. (2016) 16.
[4] Q. Wang, N. Li, B. Bolto, M. Hoang, Z. Xie, Desalination by pervaporation: a review, Desalination 387 (2016) 46–60.
[5] S. Roy, N.R. Singha, Polymeric nanocomposite membranes for next generation pervaporation process: Strategies, challenges and future prospects, Membranes (Basel) (7) 3 (53) (2017).
[6] E. Huth, S. Muthu, L. Ruff, J.A. Brant, Feasibility assessment of pervaporation for desalinating high-salinity brines, J. Water Reuse Desalin.(4) 2 (2014) 109.
[7] K. Chen, C. Xiao, H. Liu, G. Li, X. Meng, Structure design on reinforced cellulose triacetate composite membrane for reverse osmosis desalination process, Desalination 441 (2018) 35–43.
[8] M. You, J. Yin, R. Sun, X. Cao, J. Meng, Water/salt transport properties of organic/inorganic hybrid films based on cellulose triacetate, J. Membr. Sci. 563 (2018) 571–583.
[9] A. Karkooti, A.Z. Yazdi, P. Chen, M. McGregor, N. Nazemifard, M. Sadrzadeh, Development of advanced nanocomposite membranes using graphene nanoribbons and nanosheets for water treatment, J. Membr. Sci. 560 (2018) 97–107.
[10] M.S. Sri Abirami Saraswathi, A. Nagendran, D. Rana, Tailored polymer nanocomposite membranes based on carbon, metal oxide and silicon nanomaterials. A review, J. Mater. Chem. A 15 (7) (2019) 8723–8745.
[11] J. Yin, B. Deng, Polymer-matrix nanocomposite membranes for water treatment, J. Membr. Sci. 479 (2015) 256–275.
[12] J.H. Jhaveri, Z.V.P. Murthy, Nanocomposite membranes, Elsevier Inc. (57) 55 (2016).
[13] M.I. Baig, P.G. Ingole, W.K. Choi, J. Jeon, B. Jang, J.H. Moon, H.K. Lee, Synthesis and characterization of thin film nanocomposite membranes incorporated with surface functionalized Silicon nanoparticles for improved water vapor permeation performance, Chem. Eng. J. 308 (2017) 27–39.
[14] A. Khalid, A.A. Al-Juhani, O.C. Al-Hamouz, T. Laoui, Z. Khan, M.A. Atieh, Preparation and properties of nanocomposite polysulfone/multi-walled carbon nanotubes membranes for desalination, Desalination 367 (2015) 134–144.
[15] X. Zhao, J. Ma, Z. Wang, G. Wen, J. Jiang, F. Shi, L. Heng, Hyperbranched-polymer functionalized multi-walled carbon nanotubes for poly (vinylidene fluoride)

membranes: From dispersion to blended fouling-control membrane, Desalination 303 (2012) 29–38.
[16] L.Y. Yu, H.M. Shen, Z.L. Xu, PVDF–TiO_2 composite hollow fiber ultrafiltration membranes prepared by TiO_2 sol–gel method and blending method, J. Appl. Polym. Sci. 3 (113) (2009) 1763–1772.
[17] H. Zhao, L. Wu, Z. Zhou, L. Zhang, H. Chen, Improving the antifouling property of polysulfone ultrafiltration membrane by incorporation of isocyanate-treated graphene oxide, Phys. Chem. Chem. Phys. 23 (15) (2013) 9084–9092.
[18] A.M.D. Leite, L.F. Maia, E.M. Araújo, H.L. Lira, Nylon 6/Brazilian clay membranes prepared by phase inversion, J. Appl. Polym. Sci. 3 (113) (2009) 1488–1493.
[19] M.S. Jyothi, K.R. Reddy, K. Soontarapa, S. Naveen, A.V. Raghu, R.V. Kulkarni, D.P. Suhas, N.P. Shetti, M.N. Nadagouda, T.M. Aminabhavi, Membranes for dehydration of alcohols via pervaporation, J. Environ. Manage. 242 (2019) 415–429.
[20] M. Kamali, D.P. Suhas, M.E. Costa, I. Capela, T.M. Aminabhavi, Sustainability considerations in membrane-based technologies for industrial effluents treatment, Chem. Eng. J. 368 (2019) 474–494.
[21] M. Zargar, Y. Hartanto, B. Jin, S. Dai, Understanding functionalized silica nanoparticles incorporation in thin film composite membranes: interactions and desalination performance, J. Membr. Sci. 521 (2017) 53–64.
[22] F.U. Nigiz, S. Veli, N.D. Hilmioglu, Deep purification of seawater using a novel zeolite 3A incorporated polyether-block-amide composite membrane, Sep. Purif. Technol. 188 (2017) 90–97.
[23] M. Kadhom, B. Deng, Thin film nanocomposite membranes filled with bentonite nanoparticles for brackish water desalination: a novel water uptake concept, Microporous Mesoporous Mater. 279 (2019) 82–91.
[24] D. Emadzadeh, W.J. Lau, T. Matsuura, M. Rahbari-Sisakht, A.F. Ismail, A novel thin film composite forward osmosis membrane prepared from PSf-TiO_2 nanocomposite substrate for water desalination, Chem. Eng. J. 237 (2014) 70–80.
[25] Y. Li, S. Yang, K. Zhang, B. Van der Bruggen, Thin film nanocomposite reverse osmosis membrane modified by two dimensional laminar MoS2 with improved desalination performance and fouling-resistant characteristics, Desalination 454 (2019) 48–58.
[26] X. Qian, N. Li, Q. Wang, S. Ji, Chitosan/graphene oxide mixed matrix membrane with enhanced water permeability for high-salinity water desalination by pervaporation, Desalination 438 (2018) 83–96.
[27] Y. Li, S. Li, K. Zhang, Influence of hydrophilic carbon dots on polyamide thin film nanocomposite reverse osmosis membranes, J. Membr. Sci. 537 (2017) 42–53.
[28] M.A. Tofighy, Y. Shirazi, T. Mohammadi, A. Pak, Salty water desalination using carbon nanotubes membrane, Chem. Eng. J. 3 (168) (2011) 1064–1072.
[29] G. Yang, Z. Xie, M. Cran, D. Ng, S. Gray, Enhanced desalination performance of poly (vinyl alcohol)/carbon nanotube composite pervaporation membranes via interfacial engineering, J. Memb. Sci. 579 (2019) 40–51.
[30] M. Tanahashi, K. Takeda, Dispersion of nano-sized hydrophilic silica particles into various hydrophobic polymer networks, J. Nanosci. Nanotechnol. 4 (14) (2014) 3123–3136.
[31] C. Wang, Y. Xu, S. Sun, C. Zhao, Post-functionalization of carboxylic polyethersulfone composite membranes, Compos. Sci. Technol. 156 (2018) 48–60.
[32] H. Yao, S.A. Hawkins, H.J. Sue, Preparation of epoxy nanocomposites containing well-dispersed graphene nanosheets, Compos. Sci. Technol. 146 (2017) 161–168.
[33] F. Asempour, D. Emadzadeh, T. Matsuura, B. Kruczek, Synthesis and characterization of novel Cellulose Nanocrystals-based Thin Film Nanocomposite membranes for reverse osmosis applications, Desalination 439 (2018) 179–187.
[34] A. Dufresne, Cellulose nanomaterials as green nanoreinforcements for polymer nanocomposites Author for correspondence, Philos. Trans. R. Soc. A Math. Phys. Eng. Sci. (376) 2112 (2017) 20170040.
[35] A.H. Tayeb, E. Amini, S. Ghasemi, M. Tajvidi, Cellulose nanomaterials-binding properties and applications: a review, Molecules 10 (23) (2018) 1–24.
[36] L. Bai, Y. Liu, N. Bossa, A. Ding, N. Ren, G. Li, H. Liang, M.R. Wiesner, Incorporation of cellulose nanocrystals (CNCs) into the polyamide layer of thin-film composite (TFC) nanofiltration membranes for enhanced separation performance and antifouling properties, Environ. Sci. Technol. 19 (52) (2018) 11178–11187.
[37] S. Liu, Z. Low, H.M. Hegab, Z. Xie, R. Ou, G. Yang, G.P. Simon, X. Zhang, L. Zhang, H. Wang, Enhancement of desalination performance of thin-film nanocomposite membrane by cellulose nanofibers, J. Membr. Sci. 592 (2019).
[38] I. Prihatiningtyas, A. Volodin, B. Van der Bruggen, 110th anniversary: cellulose nanocrystals as organic nanofillers for cellulose triacetate membranes used for desalination by pervaporation, Ind. Eng. Chem. Res. 31 (58) (2019) 14340–14349.
[39] L. Kong, D. Zhang, Z. Shao, B. Han, Y. Lv, K. Gao, X. Peng, Superior effect of TEMPO-oxidized cellulose nanofibrils (TOCNs) on the performance of cellulose triacetate (CTA) ultrafiltration membrane, Desalination 332 (2014) 117–125.
[40] X. Chen, J. Xu, J. Lu, B. Shan, C. Gao, Enhanced performance of cellulose triacetate membranes using binary mixed additives for forward osmosis desalination, Desalination 405 (2017) 68–75.
[41] T.P.N. Nguyen, E.T. Yun, I.C. Kim, Y.N. Kwon, Preparation of cellulose triacetate/cellulose acetate (CTA/CA)-based membranes for forward osmosis, J. Membr. Sci. 433 (2013) 49–59.
[42] D.A. Cerqueira, G.R. Filho, R.M.N. de Assunção, C. da Silva Meireles, L.C. Toledo, M. Zeni, K. Mello, J. Duarte, Characterization of cellulose triacetate membranes, produced from sugarcane bagasse, using PEG 600 as additive, Polym. Bull. (60) 2–3 (2008) 397–404.
[43] B. Lam, M. Wei, L. Zhu, S. Luo, R. Guo, A. Morisato, P. Alexandridis, H. Lin, Cellulose triacetate doped with ionic liquids for membrane gas separation, Polymer 89 (2016) 1–11.
[44] J.S. Yang, H.J. Kim, W.H. Jo, and Y.S. Kang, Analysis of pervaporation of methanol-MTBE mixtures through cellulose acetate and cellulose triacetate membranes, Polymer (39) 6–7 (1998) 1381–1385.
[45] N. Bayou, O. Arous, M. Amara, H. Kerdjoudj, Elaboration and characterisation of a plasticized cellulose triacetate membrane containing trioctylphosphine oxyde (TOPO): application to the transport of uranium and molybdenum ions, Comptes Rendus Chim. 11 (13) (2010) 1370–1376.
[46] M.S. Ahmad, D.F. Mohshim, R. Nasir, H.A. Mannan, H. Mukhtar, Effect of solvents on the morphology and performance of Polyethersulfone (PES) polymeric membranes material for CO2/CH4 separation, IOP Conf. Ser. Mater. Sci. Eng. (290) 1 (2018).
[47] J. George, S.N. Sabapathi, Cellulose nanocrystals: synthesis, functional properties, and applications, Nanotechnol. Sci. Appl. 8 (2015) 45–54.
[48] J.P.F. Lagerwall, C. Schu¨tz, M. Salajkova, J.H. Noh, J.H. Park, G. Scalia, L. Bergstro¨m, Cellulose nanocrystal-based materials: from liquid crystal self-assembly and glass formation to multifunctional thin films, NPG Asia Mater. 1 (6) (2014) 1–12.
[49] R. Simha, Moderately concentrated polymer solutions, Polymer 35 (1) (1963) 1089–1098.
[50] T. Phuong, N. Nguyen, E. Yun, I. Kim, Y. Kwon, Preparation of cellulose triacetate/cellulose acetate (CTA/CA)-based membranes for forward osmosis, J. Membr. Sci. 433 (2013) 49–59.
[51] R. Jacob, H.G. Nair, J. Isac, Structural and morphological studies of nanocrystalline ceramic $BaSr_{0.9}Fe_{0.1}TiO_4$, Int. Lett. Chem. Phys. Astron. 41 (2014) 100–117.
[52] H. Bai, X. Wang, Y. Zhou, L. Zhang, Preparation and characterization of poly(vinylidene fluoride) composite membranes blended with nano-crystalline cellulose, Prog. Nat. Sci. Mater. Int. 3 (22) (2012) 250–257.
[53] S. Roy, N.R. Singha, Polymeric nanocomposite membranes for next generation pervaporation process: Strategies, challenges and future prospects, Membranes (7) 3 (2017).
[54] C. Tan, J. Peng, W. Lin, Y. Xing, K. Xu, J. Wu, M. Chen, Role of surface modification and mechanical orientation on property enhancement of cellulose nanocrystals/polymer nanocomposites, Eur. Polym. J. 62 (2015) 186–197.
[55] V. Baheti, J. Militky, M. Marsalkova, Polyvinyl alcohol-modified pithecellobium clypearia benth herbal residue fiber polypropylene composites, Polym. Compos. 1 (37) (2016) 915–924.
[56] M.G. Aguayo, A. Fernández Pérez, G. Reyes, C. Oviedo, W. Gacitúa, R. Gonzalez, O. Uyarte, Isolation and characterization of cellulose nanocrystals from rejected fibers originated in the Kraft Pulping process, Polymers (Basel) 10 (2018) 10.
[57] N. Wang, E. Ding, R. Cheng, Thermal degradation behaviors of spherical cellulose nanocrystals with sulfate groups, Polymer (Guildf) 12 (48) (2007) 3486–3493.
[58] Q. Zhang, C.D. Vecitis, Conductive CNT-PVDF membrane for capacitive organic fouling reduction, J. Membr. Sci. 459 (2014) 143–156.
[59] S.M.J. Zaidi, F. Fadhillah, Z. Khan, A.F. Ismail, Salt and water transport in reverse osmosis thin film composite seawater desalination membranes, Desalination 368 (2015) 202–213.
[60] D. Wu, A. Gao, H. Zhao, X. Feng, Pervaporative desalination of high-salinity water, Chem. Eng. Res. Des. 136 (2018) 154–164.
[61] B.M. Fabuss, A. Korosi, Vapor pressures of binary aqueous solutions of NaCl, KCl, Na_2SO_4 and $MgSO_4$ at concentrations and temperatures of interest in desalination processes, Desalination 2 (1) (1966) 139–148.
[62] I. Prihatiningtyas, G.A. Gebreslase, B. Van der Bruggen, Incorporation of Al_2O_3 into cellulose triacetate membranes to enhance the performance of pervaporation for desalination of hypersaline solutions, Desalination 474 (2020) 114198.
[63] H.K. Lonsdale, U. Merten, R.L. Riley, Transport properties of cellulose acetate osmotic membranes, J. Appl. Polym. Sci. (9) 4 (1965) 1341–1362.
[64] Y.P. Kuznetsov, E.V. Kruchinina, Y.G. Baklagina, A.K. Khripunov, O.A. Tulupova, Deep desalination of water by evaporation through polymeric membranes, Russ. J. Appl. Chem. 5 (80) (2007) 790–798.
[65] M. Naim, M. Elewa, A. El-Shafei, A. Moneer, Desalination of simulated seawater by purge-air pervaporation using an innovative fabricated membrane, Water Sci. Technol. 5 (72) (2015) 785–793.

Effect of solvent on the morphology and performance of cellulose triacetate membrane/cellulose nanocrystal nanocomposite pervaporation desalination membranes

ORIGINALITY REPORT

21%	2%	21%	2%
SIMILARITY INDEX	INTERNET SOURCES	PUBLICATIONS	STUDENT PAPERS

MATCH ALL SOURCES (ONLY SELECTED SOURCE PRINTED)

11%

★ Indah Prihatiningtyas, Alexander Volodin, Bart Van der Bruggen. " Cellulose Nanocrystals as Organic Nanofillers for Cellulose Triacetate Membranes Used for Desalination by Pervaporation ", Industrial & Engineering Chemistry Research, 2019

Publication

Exclude quotes	On	Exclude matches	< 2%
Exclude bibliography	On		